Published in final edited form as:

Cell Rep. 2019 June 11; 27(11): 3107–3116.e3. doi:10.1016/j.celrep.2019.05.056.

Presynaptic Expression of LRIT3 Transsynaptically Organizes the Postsynaptic Glutamate Signaling Complex Containing TRPM1

Nazarul Hasan[1,6], **Gobinda Pangeni**[2,6], **Catherine A. Cobb**[1], **Thomas A. Ray**[1], **Emily R. Nettesheim**[4], **Kristina J. Ertel**[4], **Daniel M. Lipinski**[4,5], **Maureen A. McCall**[2,3], and **Ronald G. Gregg**[1,2,3,7,*]

[1]Department of Biochemistry and Molecular Genetics, University of Louisville, Louisville, KY 40292, USA

[2]Department of Ophthalmology and Visual Sciences, University of Louisville, Louisville, KY 40292, USA

[3]Department of Anatomical Sciences and Neurobiology, University of Louisville, Louisville, KY 40292, USA

[4]Department of Ophthalmology and Visual Sciences, Medical College of Wisconsin, Milwaukee, WI 53226, USA

[5]Nuffield Laboratory of Ophthalmology, University of Oxford, Oxford OX3 9DU, UK

[6]These authors contributed equally

[7]Lead Contact

SUMMARY

Throughout the CNS, interactions between pre- and postsynaptic adhesion molecules establish normal synaptic structure and function. Leucine-rich repeat (LRR) domain-containing proteins are a large family that has a diversity of ligands, and their absence can cause disease. At the first retinal synapse, the absence of LRIT3 expression leads to the disassembly of the postsynaptic glutamate signaling complex (signalplex) expressed on depolarizing bipolar cell (DBC) dendrites. The prevalent view is that assembly of the signalplex results from direct post-synaptic protein:protein interactions. In contrast, we demonstrate that LRIT3 is expressed presynaptically, in rod photoreceptors (rods), and when we restore LRIT3 expression in *Lrit3*$^{-/-}$ rods, we restore expression of the postsynaptic glutamate signalplex and rod-driven vision. Our results demonstrate

*Correspondence: ron.gregg@louisville.edu.

AUTHOR CONTRIBUTIONS

Conceptualization, R.G.G., M.A.M., and N.H.; Investigation, N.H., G.P., C.A.C., T.A.R., K.J.E., and E.R.N.; Writing – Original Draft, R.G.G.; Writing – Review & Editing, R.G.G. and M.A.M.; Funding Acquisition, R.G.G., M.A.M.,N.H., and D.M.L.; Supervision, R.G.G., M.A.M., and D.M.L.

SUPPLEMENTAL INFORMATION

Supplemental Information can be found online at https://doi.org/10.1016/j.celrep.2019.05.056.

DECLARATION OF INTERESTS

The authors declare no competing interests.

that, in the retina, the LRR-containing protein LRIT3 acts as a transsynaptic organizer of the postsynaptic complex required for normal synaptic function.

Graphical Abstract

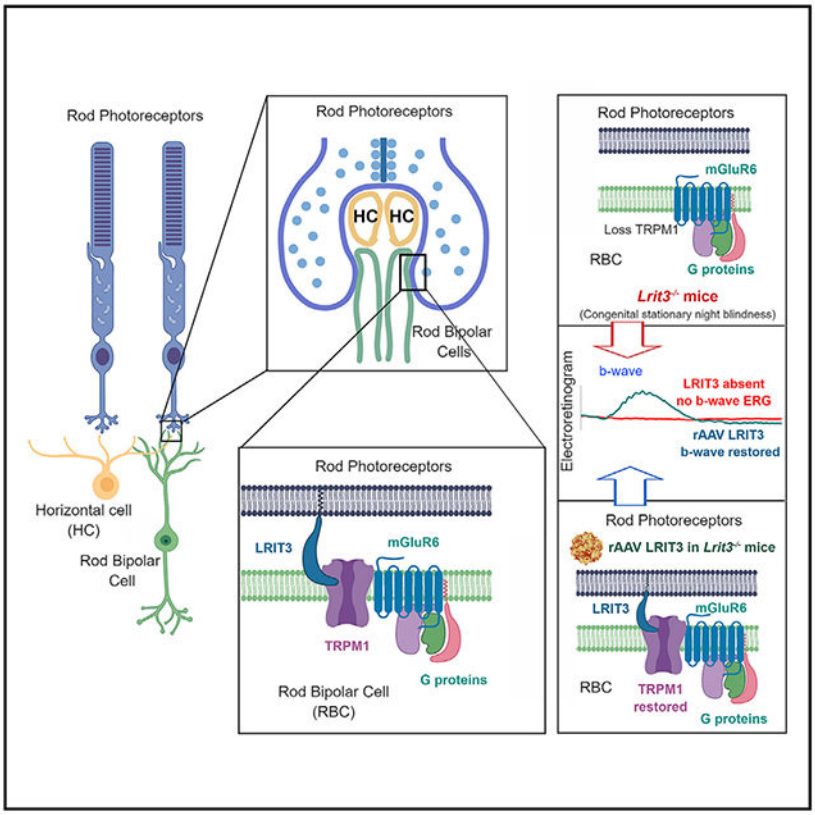

In Brief

The leucine-rich repeat-containing protein LRIT3 is required for dim-light vision and postsynaptic signalplex assembly. Hasan et al. show that LRIT3 is expressed in rod photoreceptors and acts transsynaptically to localize the TRPM1 channel in the postsynaptic membrane. LRIT3 expression in knockout mice restores retinal function.

INTRODUCTION

Synaptic function requires the precise alignment of pre- and postsynaptic elements, including alignment of signaling molecules that govern neurotransmitter release and its detection. This exquisite precision is achieved by coordinated expression of a large number of proteins from several adhesion molecule gene families. One of these, the leucine-rich repeat (LRR) family, has several hundred members, and for many their LRR domains are extracellular and interact transsynaptically with postsynaptic binding partners. They are expressed throughout the CNS, where they are important organizers of synapses and synaptic function (Schroeder and de Wit, 2018). Many LRRs have minimal or no

intracellular domain, which indicates that they act as co-receptors to organize specific signaling molecules.

At the first retinal synapse, four LRR-containing proteins, ELFN1, LGN2, Nyctalopin, and LRIT3, have been identified and the absence of their expression disrupts synaptic structure and/or function. The absence of ELFN1, expressed in rods, eliminates localization of the presynaptic calcium channels required for neurotransmitter release (Cao et al., 2015; Wang et al., 2017). The absence of LGN2, expressed in horizontal cells (HCs) post-synaptic to photoreceptors, disrupts synaptic structure (Soto et al., 2013, 2018). The absence of Nyctalopin, expressed in postsynaptic depolarizing rod and cone bipolar cells (BCs; collectively light onset [ON] BCs), disrupts trafficking and/or clustering of TRPM1 in their postsynaptic dendritic tips, without alteration of synaptic structure (Ball et al., 2003; Pardue et al., 2001), and causes complete congenital stationary night blindness (cCSNB; Bech-Hansen et al., 2000; Gregg et al., 2003; Pusch et al., 2000). The absence of LRIT3 disrupts trafficking of TRPM1 (Neuillé et al., 2015), which is the non-specific cation channel that leads to postsynaptic DBC depolarization. LRIT3 also is required for Nyctalopin expression at the dendritic tips of DBCs (Hasan et al., 2018). Taken together these results predicted that the LRR-containing proteins LRIT3 and Nyctalopin may interact postsynaptically and serve to organize postsynaptic receptor assembly in DBCs, but not synapse formation and/or maintenance.

In contrast to this expectation, we show that the trafficking and postsynaptic localization of TRPM1 in rod BCs (RBCs) depend on presynaptic expression of LRIT3 in rods. Finally, we show that restoration of LRIT3 expression in rods selectively restores scotopic, but not photopic, retinal function in RBCs and retinal ganglion cells (RGCs). This restoration of scotopic visual function results from restored insertion of TRPM1 into the dendritic tips of RBCs. Together, these data show that an LRR family protein, LRIT3, acts in a transsynaptic manner and organizes key post-synaptic RBC signaling complex (signalplex) components, in particular TRPM1.

RESULTS

Immunohistochemistry and confocal microscopy show that LRIT3 expression is confined to the retinal outer plexiform layer (OPL) and is co-localized with the ON BC signalplex proteins mGluR6, TRPM1, and GPR179 (Neuillé et al., 2017; Ray, 2013). In *Lrit3*^{nob6} (Neuillé et al., 2015) and *Lrit3*$^{-/-}$ (Hasan et al., 2018; Ray, 2013) mice, the loss of LRIT3 results in the loss of TRPM1 expression, suggesting that the two molecules may interact. To determine if LRIT3 is expressed pre- and/or postsynaptically, we used *in situ* hybridization. We found that *Lrit3* mRNA was expressed in the outer nuclear layer (ONL), where photoreceptor cell bodies are located, with some relatively sparse expression in the inner nuclear layer (INL) (Figure 1A). Consistent with the known expression of mGluR6 in ON BCs, labeling for *Grm6* mRNA was confined to the outer portion of the INL (Figure 1A). Given this difference in expression and the immunohistochemical results showing TRPM1 localization depends on LRIT3 expression, we hypothesized that LRIT3 expression localized TRPM1 to ON BC dendritic tips by a transsynaptic mechanism.

To investigate this idea, we devised a recombinant adeno-associated virus (rAAV) strategy to restore LRIT3 expression to rods of *Lrit3*$^{-/-}$ mice and examine the effect on retinal function. The construct used a human rhodopsin (RHO) promoter to drive expression in photoreceptors (Mussolino et al., 2011), and a schematic of our construct is shown in Figure 1B. Four to 8 weeks after intravitreal injection of rAAV RHO::Lrit3 into *Lrit3*$^{-/-}$ mice, we used immunohistochemistry to determine the impact of virally mediated expression of LRIT3 in rods on RBC signalplex structure and function.

rAAV-Mediated Expression of LRIT3 in *Lrit3*$^{-/-}$ Rods Restores Trafficking of TRPM1 to the Postsynaptic RBC Dendrites

RBCs initiate light signaling through a transduction cascade that begins with glutamate binding to mGluR6 and culminates with modulation of the TRPM1 channel. Both mGluR6 and TRPM1 are expressed in RBCs and cone ON BCs, and both co-localize with LRIT3, among other DBC signalplex proteins (Neuillé et al., 2015; Ray, 2013). In *Lrit3*$^{-/-}$ retinas, mGluR6 expression is normal in rod synapses but absent from cone terminals (Figure 1Cii), and TRPM1 expression is absent from the dendritic tips of ON BCs (Figure 2) but remains in the cell bodies, where it is localized to the endoplasmic reticulum (Agosto et al., 2018).

To determine if LRIT3 expression in the rods restored its expression to the OPL, we examined its localization relative to mGluR6 and TRPM1 in *Lrit3*$^{-/-}$ retinas infected with rAAV RHO::Lrit3. In control retinas, there is 100% co-localization of LRIT3 and mGluR6 puncta (Figure 1Ci). In transverse sections, rod synapses appear as puncta because rod axon terminals have a single invaginating complex of two rod BC and two HC dendrites. In contrast, cone synapses appear as elongated profiles because their large axon terminals contain multiple invaginations of ON BCs and HCs (Figure 1Ci, arrowheads at bottom of the OPL). The staining for mGluR6 at the axon terminals of *Lrit3*$^{-/-}$ rods is similar morphologically to controls, and the pattern of staining is indistinguishable (Figures 1Ci and Cii). In contrast, the axon terminals of the *Lrit3*$^{-/-}$ cones lack expression of mGluR6 (Figure 1Cii). The LRIT3 expressed in *Lrit3*$^{-/-}$ rods by rAAV RHO::Lrit3 correctly co-localizes with many mGluR6 puncta (Figures 1Ciii and 1E), and when present, it always co-localizes with mGluR6. Puncta stained only for mGluR6 (green) represent synapses of rods uninfected by rAAV RHO::Lrit3.

To examine LRIT3 expression over larger areas, we imaged whole-mount retinas at the level of the OPL after immuno-staining for mGluR6 and LRIT3. In controls (Figure 1Di), LRIT3 profiles for rod (greenish-white puncta) and cone (purple clusters indicated with dashed circles) synapses are readily distinguished. Here too, it is evident that there is 100% co-localization of mGluR6 and LRIT3 in both rod and cone terminals. The difference in the color of the two types of profiles in the merged images suggests that the ratio of LRIT3 to mGluR6 in rod versus cone synapses differs. Specifically, there is more LRIT3 relative to mGluR6 in cone terminals compared with that in rod terminals. In the rAAV RHO::Lrit3-infected *Lrit3*$^{-/-}$ retinas, mGluR6 and the restored LRIT3 expression are punctate, consistent with expression in rod synapses (Figure 1Dii). There is no evidence of LRIT3 expression in the cone terminal, as expected, given the use of the RHO promoter. Similar to the data in transverse sections, some mGluR6 puncta co-localize with LRIT3 and others do not (Figure

1Dii). We quantified the percentage of puncta in which LRIT3 and mGluR6 co-localized in ten pieces of retina from five *Lrit3*$^{-/-}$ mice injected with rAAV RHO::Lrit3 (Figure 1F). In control mice, there was 100% co-localization of mGluR6 and LRIT3. In rAAV RHO::Lrit3-treated retinas, the percentage of mGluR6 to LRIT3 co-localization varied from 39.5% to 73% (Figure 1E; n = 5 eyes). In *Lrit3*$^{-/-}$ mice, there was 0% co-localization, because LRIT3 expression was absent (Figures 1Cii and 1E).

To form a functional synapse, expression of LRIT3 in rods must restore its expression and co-localization with the RBC signalplex, specifically mGluR6. In controls, there is 100% colocalization of LRIT3 and TRPM1 (Figure 2Ai), and both are absent from dendritic tips of the *Lrit3*$^{-/-}$ retinas (Figure 2Aii). In rAAV RHO::Lrit3-injected *Lrit3*$^{-/-}$ retinas, TRPM1 punctate expression is restored to the OPL, and there is 100% co-localization with expression of LRIT3 (Figure 2Aiii). To examine this further, we triple-labeled a subset of retinas for mGluR6, TRPM1, and LRIT3. All LRIT3 puncta that co-localized with mGluR6 also co-localized with TRPM1 (Figure 2B), and there were many puncta that stained only for mGluR6 (Figure 2B, green puncta in merged images). These data show that LRIT3 expression in rods is necessary and sufficient to restore normal expression of TRPM1 to the tips of RBCs. The impact of LRIT3 loss on several known RBC signalplex components is shown schematically in Figure 2C. The loss of LRIT3 causes a loss of TRPM1 and Nyctalopin, and its expression in rods restores TRPM1 expression to the dendritic tips of the RBCs. This restoration is analogous to a previous study in which we rescued Nyctalopin expression in RBCs of *Nyx*^{nob} mice and showed that TRPM1 expression was restored as well as function (Scalabrino et al., 2015). The major and surprising result here is that LRIT3 can restore TRPM1 expression to the dendrites of RBCs in a transsynaptic manner.

rAAV-Mediated LRIT3 Expression in Rods Restores the ERG b-Wave in *Lrit3*$^{-/-}$ Mice

We next examined if rescue of TRPM1 to the RBCs by expressing LRIT3 in rods restored function using the electroretinogram (ERG) and RGC recordings. *Lrit3*mice retain a normal a-wave but lack b-waves under both scotopic and photopic conditions (Figure 3; Hasan et al., 2018; Neuillé et al., 2014; Ray, 2013). To assess the effect and efficiency of expression of LRIT3 in rods, we performed full-field ERGs in the same eyes in which we restored LRIT3 expression to ~50% of the rods in the *Lrit3*$^{-/-}$ mice (Figure 1E). We assessed ERG responses in eight *Lrit3*$^{-/-}$ eyes injected with rAAV RHO::Lrit3 and three control eyes injected with rAAV RHO::GFP (Figure 3). We show representative scotopic (Figure 3A) and photopic (Figure 3B) ERG responses from an injected eye in each condition, as well as a control *Lrit3*$^{-/-}$ mouse. Summary data for all eyes for both scotopic (Figure 3C) and photopic (Figure 3D) conditions show that restoration of LRIT3 expression in *Lrit3*$^{-/-}$ eyes partially restores the scotopic b-wave compared with normal controls injected with rAAV RHO::GFP ($p_{adj} < 0.003$ for all flash intensities, t test, Bonferroni corrected). The extent of b-wave rescue in rAAV RHO::LRIT3 eyes was significantly less than for wild-type (WT) ($p_{adj} < 0.01$ for all flash intensities, two-way ANOVA, Bonferroni corrected) consistent with the ~50% infection of rods in the rAAV RHO::LRIT3-treated animals. The injection of rAAV RHO::Lrit3 did not rescue the photopic b-wave (Figure 3D). The red and blue dashed lines (Figures 3C and 3D) represent the fact that the b-wave is absent in *Lrit3*$^{-/-}$ mice. The extent of the rescue of the b-wave varied across treated *Lrit3*$^{-/-}$ mice, but on average,

treatment resulted in ~50% recovery of the b-wave amplitude (Figure 3C). The presence of the b-wave oscillatory potentials in the single animal traces (Figure 3A) also suggests restoration of inner retinal function. The failure to restore a photopic response is consistent with the expression pattern of the RHO promoter primarily in rods. On the basis of these data, we conclude that infection with rAAV RHO::Lrit3 restores LRIT3 expression to infected rods, which restores TRPM1 expression in connecting RBCs and rescues their function as assessed by the scotopic ERG.

rAAV-Mediated LRIT3 Expression in Rods Restores Normal ON Responses in *Lrit3*$^{-/-}$ RGCs

In control mouse retina, short-latency RGC responses (latency < 500 ms) are evoked at light onset (ON), light offset (OFF), and both light on and off (ON/OFF, Figure 4Ai). In contrast, all mouse models of cCSNB (*Grm6*$^{-/-}$, *Trpm1*$^{-/-}$, *Gpr179*^{nob5}, *Nyx*^{nob}, *Lrit3*^{nob6}, and *Lrit3*$^{-/-}$), which lack function through the ON BCs, have ON RGCs that lack normal-latency ON responses to stimuli (Demas et al., 2006; Neuillé et al., 2017; Peachey et al., 2017; Rentería et al., 2006). Instead, the responses of these cCSNB RGCs to ON are significantly delayed (>500 ms time to peak [TTP]; Peachey et al., 2017) and arise from crossover inputs from the OFF to the ON pathway (Rentería et al., 2006) and are referred to as dON (Figure 4Aii; Table S1).

We independently assessed the spiking responses of RGCs in the same rAAV RHO::Lrit3-infected *Lrit3*$^{-/-}$ retinas assessed in the immunohistochemical and ERG experiments (Figures 1, 2, and 3) using a multi-electrode array (MEA). We recorded from two pieces of retina from five eyes that had partial scotopic b-wave restoration and examined both rod- and cone-driven responses to flashes from 276 control, 377 *Lrit3*$^{-/-}$ and 476 rAAV RHO::Lrit3-treated *Lrit3*$^{-/-}$ RGCs. A unique feature of the *Lrit3*$^{-/-}$ retina is that the majority of RGCs lack a visually evoked response (Hasan et al., 2018). Although they retain spontaneous activity, 92.6% and 61.3% of the RGCs are non-responsive (NR) under scotopic and photopic stimuli, respectively (Figure 4C; Table S1), compared with 28% and 2% in controls. The number of NR RGCs decreased under scotopic conditions in the rAAV RHO::Lrit3-injected *Lrit3*$^{-/-}$ retinas compared with uninjected *Lrit3*$^{-/-}$ controls (Figure 4Ci; 70% versus 92.6%, $p < 0.01$), although there were still more NR RGCs than controls (70% versus 28%; $p < 0.01$). Under scotopic conditions, ~40% of control RGCs have short-latency responses to ON, and there are no long latency responses (Figure 4Bi). In the *Lrit3*$^{-/-}$ retinas, there are very few responsive cells, but those with ON responses have delayed (>500 ms after stimulus onset) TTP (Figure 4Bii). RGCs in rAAV RHO::Lrit3-injected *Lrit3*$^{-/-}$ retinas have a broad range of TTP, either short-latency (<500 ms, 96 of 476) or delayed (dON) (29 of 476) responses (Figures 4Aiii, 4Biii, and 4Ci) encompassing those present in control and *Lrit3*$^{-/-}$ (Figure 4B). These data are consistent with the partial recovery of the scotopic ERG b-wave and LRIT3 expression in some but not all rods.

To verify that the rescued rAAV RHO::Lrit3 RGC ON responses represent restoration of the mGluR6 signalplex in the rod pathway, we recorded the scotopic responses of these same RGCs in the presence of L-AP4, to block mGluR6-initiated signaling (Slaughter and Miller, 1981). This experiment shows that L-AP4 eliminates the short-latency ON responses in both control and in rAAV RHO::Lrit3-injected *Lrit3*$^{-/-}$ retinas (Figures 4Di and 4Ei), which

returned to normal after washout (Figures 4Dii and 4Eii; control [n = 26] versus rRHO::Lrit3-injected *Lrit3*$^{-/-}$ [n = 44]; $p_{adj} > 0.4$, Ringer's versus wash for both groups, repeated-measures ANOVA, Bonferroni corrected). These data confirm that short-latency ON RGC responses in the rAAV RHO::Lrit3-treated *Lrit3*$^{-/-}$ retinas arise because of the rescued expression of LRIT3 and the restoration of a functional mGluR6 to TRPM1 transduction cascade.

We also examined the responses of RGCs in the three groups under photopic conditions. Under cone-driven conditions, almost all RGCs (98% [208 of 210]) in normal control mice are visually responsive (39% ON, 48% ON/OFF, 11%OFF; Figure 4; Table S1). In contrast, only 38% (146 of 377) of *Lrit3*$^{-/-}$ RGCs are visually responsive, and these have only dON (4 of 146) or OFF (142 of 146) responses (Figure 4Cii). In the rAAV RHO::Lrit3-treated *Lrit3*$^{-/-}$ retinas, 35.5% (169 of 476) of the RGCs were responsive (7 ON, 2 ON/OFF, 1 d ON, 12 d ON/OFF, 147 OFF) under cone-driven conditions. In this group, we found 7 RGCs (1.5% [7 of 476]) distributed across several retinas that had normal-latency photopic ON responses. The presence of these cells did not correlate with the number of normal ON responses at scotopic levels. Despite this rescue, the peak firing rates of these ON RGCs were lower than normal controls (21.9 ± 3.8 [n = 8] versus 36.5 ± 1.3 [n = 173] spikes/s, $p < 0.05$). We propose these cells arise because of ectopic expression of LRIT3 in a very small percentage, or at low levels in a few, cones infected with rAAV RHO::Lrit3. This number and/or level is low because we did not identify any LRIT3 expression in cone terminals in whole mounts of the rAAV RHO::Lrit3-injected *Lrit3*$^{-/-}$ retinas (see Figures 1 and 2). However, some low-level expression is consistent with the fact that the human RHO promoter is leaky and can express in cones (Allocca et al., 2007).

The number of functional rod to RBC connections restored was positively correlated with the amplitude of the ERG b-wave and the percentage of RGCs that have normal ON responses (Figure S1). Taken together, our results show that expression of LRIT3 in rods of *Lrit3*$^{-/-}$ mice rescues the RBC response and many ON RGCs. Thus, it is clear that LRIT3 acts as a presynaptic rod photoreceptor protein and transsynaptically organizes TRPM1 localization to the RBC signalplex.

rAAV RHO::Lrit3 Treatment at P35 Restores TRPM1 Expression and Scotopic Function in Adult *Lrit3*$^{-/-}$ Retinas

The above results show that introduction of LRIT3 protein expression into rods of P5 mice restores rod-driven function. At the time of injection (P5), only the ganglion cells have differentiated, and the rest of the retina is a neuroblast layer, which gradually laminates and differentiates (Hoon et al., 2014). Synapses between photoreceptors and BCs mature around the time of eye opening (~P11). If gene therapy is an option for cCSNB patients, introduction of LRIT3 would occur at later developmental stages, when the retina is mature. As such, we tested if intravitreal injection of rAAV RHO::Lrit3 into mature (P35) mouse retina also could restore rod-driven function and localization of TRPM1 to RBC dendritic tips.

Immunohistochemical analyses of retinal whole mounts shows that injections of the rAAV RHO::Lrit3 at P35 restores LRIT3 expression in the OPL of *Lrit3*$^{-/-}$ (Figure 5A), with a

pattern similar to P5 injection (Figure 1), although to far fewer rods than for the P5 injections (8.5% ± 1.3% versus 56% ± 6.6%, $p < 0.002$; Figure 5B). LRIT3 puncta are clearly visible, and 100% co-localize with TRPM1 puncta. A subset of LRIT3 and TRPM1 puncta is highlighted by dashed circles for easy comparison (Figure 5A).

ERG analyses 5 weeks after injection of the *Lrit3*$^{-/-}$ mice at P35 shows that a scotopic ERG response is evident in both the scotopic flash series for a single animal (Figure 5C) and for all treated retinas compared with *Lrit3*$^{-/-}$ control (Figure 5C) at the dimmest flash that isolates rod function (−3.6 log cd/m^2; Figure 5E). The lack of measurable b-waves at scotopic stimuli intensities from −2.4 to 1.4 log cd s/m^2 represents the decreased sensitivity of the retina and the low fraction (8.5% ± 1.3%) of rods expressing LRIT3, and consequently TRPM1, when virus was injected at P35, compared to P5 (56% ± 6.6% rods infected). A representative photopic flash series is shown for a single P35-injected mouse, and as expected, there is no functional rescue, because expression of LRIT3 is directed only to rods (Figure 5D). The photopic ERGs for all mice were indistinguishable from *Lrit3*$^{-/-}$ recordings (data not shown). Finally, we quantified the peak b-wave amplitude of WT and age-matched rAAV RHO::Lrit3-injected and uninjected *Lrit3*$^{-/-}$ ERGs (Figure 5F). Again, WT eyes produce a larger amplitude b-wave than the rAAV RHO::Lrit3-injected eyes ($p < 0.001$), which have larger amplitudes than mature *Lrit3*$^{-/-}$ mice ($p < 0.005$; Figure 5F).

DISCUSSION

Our results show LRIT3 is expressed in photoreceptors and that rAAV-mediated expression of LRIT3 in *Lrit3*$^{-/-}$ rods rescues expression of TRPM1 in RBCs. In our datasets, rescue appears to be more efficient in eyes treated at P5 compared with P35. Although the reason remains unclear, it could be related to the timing of LRIT3 expression. For example at P5 synapses are immature, outer retinal cells are differentiating, and pre- and postsynaptic signalplexes are being organized. These processes are complete by P35 (see review by Hoon et al., 2014). Alternatively, AAV infection itself may favor young compared with mature retinas. Indeed, our previous study of the rescue of Nyctalopin in ON BCs showed that early (P2) viral treatment was much more efficient at restoring expression than in adults (Scalabrino et al., 2015).

Regardless, of how restoration is controlled, the expression of LRIT3 in presynaptic rods restores the localization and function of TRPM1 to the postsynaptic signalplex, demonstrating that it functions in a transsynaptic mechanism. LRIT3 is a member of a large family of LRR-containing proteins that are known to be involved in transsynaptic functions. These include NGLs, LRRTMs, Slitrks, SALMs, and FLRTs, and most act transsynaptically to organize the structure and composition of synapses and, as a consequence, have been implicated in diseases such as autism, schizophrenia, and Alzheimer’s disease (see review by Schroeder and de Wit, 2018). In many studies of these individual proteins, the focus has been on functions such synaptic strength, numbers of spine, synapse density, and synaptic plasticity; thus, the underlying molecular mechanisms are poorly understood.

The level of complexity was demonstrated by Schroeder et al. (2018), who examined the function of three LRRs, FLRT2, LRRM1, and Slitrk1, that are expressed postsynaptically at

CA1 pyramidal cell inputs and transsynaptically organize the properties of their synapses. The expression pattern and function of each depended on the specific synapses in which they were expressed. Here we show that presynaptic LRIT3 expression in rods is required for TRPM1 insertion into the postsynaptic RBCs membrane. In rods LRIT3 also is required for the postsynaptic expression of Nyctalopin (Hasan et al., 2018). In contrast, at the cone to cone bipolar synapse LRIT3 is required for not only for expression of Nyctalopin and TRPM1, but also for mGluR6, GPR179, and thus the RGS complex (Neuillé et al., 2015; Hasan et al., 2018; Ray, 2013). Thus, organization of the cone synapse appears more complex and may require expression of LRIT3 pre- and postsynaptically and also is likely to require other unidentified interacting partners that may not be needed at the rod synapse.

Finally, although the detailed protein:protein interactions between LRIT3 and its postsynaptic partners in RBCs remain to be established, we hypothesize that this transsynaptic mechanism includes an interdependent interaction with not only TRPM1 but also Nyctalopin, another LRR-containing protein (Bech-Hansen et al., 2000; Gregg et al., 2003; Pusch et al., 2000). Our rationale is that we know that TRPM1 dendritic expression depends on expression of Nyctalopin (Pearring et al., 2011), and that Nyctalopin expression depends on LRIT3 (Hasan et al., 2018), suggesting a complex interaction profile.

In the cone pathway, we do not know whether LRIT3 is presynaptic, expressed in cone photoreceptors, or postsynaptic, expressed in ON cone BCs, or both. Our results show a small number of rAAV RHO::Lrit3 ON RGCs with normal response latency. In contrast, we have never seen normal-latency ON responses in our survey of more than 1,000 RGCs from *Lrit3*$^{-/-}$ retinas (unpublished observations). This result suggests that LRIT3 expression in cones can restore normal cone ON BC function, even though the disruption to the cone ON BC signalplex in the *Lrit3*$^{-/-}$ retina is more severe (loss of all signalplex components) than in RBCs (Neuillé et al., 2015; Ray, 2013).

Another LRR-containing protein, ELFN1, which is expressed by rods has been proposed to have transsynaptic function and to interact with mGluR6 (Cao et al., 2015; Sarria et al., 2018; Ueno et al., 2018). Unlike the *Lrit3*$^{-/-}$ retina, the entire rod to RBC synapse in the *Elfn1*$^{-/-}$ retina is severely disrupted. ELFN1 interacts with the voltage-gated calcium channel (VDCC) subunit $\alpha_2\delta_4$ (CACND4) (Cao et al., 2015; Wang et al., (2017). The $\alpha_2\delta_4$ subunit combines with α_{1F} (CACNA1F) and β_2 (CACNB2) to govern both normal photoreceptor synaptic function and development and neurotransmitter release from rods and cones (Ball et al., 2002; Bech-Hansen et al., 1998; Chang et al., 2006; Katiyar et al., 2015; Mansergh et al., 2005; Strom et al., 1998; Kerov et al., 2018; see review by Waldner et al., (2018). Although a direct transsynaptic protein:protein interaction of ELFN1 and mGluR6 *in vivo* is possible, the breakdown of presynaptic structure and function is an equally plausible explanation for the absence of mGluR6 expression. A direct interaction of ELFN1 and mGluR6 also is discordant with immuno-electron microscopy (EM) studies that indicate mGluR6 is located 100 nm away from the photoreceptor transmitter release sites (Vardi et al., 2000), and the lack of overlap between mGluR6 and CACNA1F in many immunohistochemical studies. In contrast, we show that LRIT3 has a clear transsynaptic function to stabilize insertion of the TRPM1/Nyctalopin complex in the postsynaptic RBC, and its absence does not disrupt synaptic structure.

This lays the groundwork for study of other LRR-containing proteins in organizing other synaptic complexes throughout the retina and the rest of the nervous system. These data also show that a gene therapy approach, in which the gene is expressed presynaptically early in development as well as in adults, can restore postsynaptic signalplex function of RBCs *in vivo*. The greater improvement in the restoration of the b-wave in *Lrit3*$^{-/-}$ eyes that were treated at P5 compared with intravitreal injection into adult (P35) eyes suggests that optimization of virus coat, delivery method (intravitreal versus subretinal), and titer will be required to establish the viability of an effective gene therapy.

STAR★METHODS

CONTACT FOR REAGENT AND RESOURCE SHARING

Further information and requests for resources and reagents should be directed to and will be fulfilled by the Lead Contact, Ronald Gregg (ron.gregg@louisville.edu).

EXPERIMENTAL MODEL AND SUBJECT DETAILS

All procedures were performed in accordance with The Association for Research in Vision and Ophthalmology (ARVO) policies on the use of animals in research, and the University of Louisville Institutional Animal Care Use Committee. Animals were housed in the University of Louisville AALAC approved facility under a 12 h/12 h light/dark cycle with continuous access to food and water. Mice of both sexes were used. No mice showed abnormal health or immune abnormalities. The *Lrit3*^{em1Rgg}, hereafter referred to as *Lrit3*$^{-/-}$, were backcrossed to C57BL/6J mice (Jackson Labs) for at least 10 generations. Adult animals were analyzed and where appropriate specific ages are given in the text.

In some experiments we transduced retina with rAAV RHO::GFP, these are designated Control rAAV RHO::GFP. Data from these animals was indistinguishable from controls (C57BL/6J mice). For all procedures, mice were anesthetized with intraperitoneal injections of ketamine/xylazine solution (127/12 mg/kg, respectively) diluted in normal mouse Ringer's.

METHOD DETAILS

Antibodies—The LRIT3 and TRPM1 antibodies were used at 1:1000 dilution. Other antibodies: anti-mGluR6 (1:1000, gift Dr. Kiril Martemyanov; Cao et al., 2011), Secondary antibodies were Alexa Fluor 488 Donkey anti-sheep (1:1000), Alexa Fluor 488 Donkey anti-rabbit (1:1000), Alexa Fluor 647 Donkey anti-rabbit (1:1000) and Donkey anti-guinea pig Cy3 conjugated (1:1000).

Retina preparation—After death, the eyes were enucleated and the cornea and lens removed. The retina was dissected in 0.1M PB and fixed for 15-60 min in PBS containing 4% paraformaldehyde, washed in PBS for 5 min, and cryoprotected in a graded series of sucrose solutions (5, 10, 15 and 20% in PBS) and finally in OCT:20% sucrose (2:1). Retinas were embedded and frozen in OCT:20% sucrose (2:1) in a liquid nitrogen cooled isopentane bath. Transverse retinal sections (18 μm) were cut on a cryostat (Leica Biosystems, Buffalo

Grove, IL), mounted on Superfrost Plus slides (Thermo Fisher Scientific, Waltham, MA), and stored at −80°C.

RNA *in situ* hybridization—We used a fluorescence based *in situ* hybridization system to visualize target transcripts in fixed retinal sections as described by the manufacturer (RNAScope®; ACDBio, Newark, CA). Tissue sections, mounted onto glass slides were baked overnight at 60°C and incubated in pre-treatment buffer 2 for 4 min at a temperature of 90-105°C, without active boiling. Pre-treatment buffer 3 was applied for 12 min, and 50 μL of FastRed added to each slide. Target probes were synthesized by ACDBio for transcripts encoded by *Lrit3* and *Grm6* (Genbank: NM_173372.2, 1001-2020bp). Positive and negative control probes were *Polr2a* (RNA polymerase II subunit A) and *DapB* (a bacterial gene), respectively. Slides were coverslipped, sealed with nail polish and imaged on an Olympus FV1000 confocal microscope.

Immunohistochemistry—Immunohistochemistry methods have been described previously (Hasan et al., 2016). Briefly, slides were warmed and sections dried at 37°C for 30 min, rinsed in PBS for 5 min, and PBX (PBS + 0.5% Triton X-100) for 5 min. Sections were blocked by incubated in blocking buffer (PBX + 5% normal donkey serum) for 1 h. Antibodies were added to blocking buffer and incubated with sections overnight at room temperature. Primary antibody was removed by washing 3×10 min in PBX, then secondary antibody was added in blocking buffer for 1 h. Finally, sections were washed 2 times in PBX and 1 time in PBS, each for 10 min, then coverslips were mounted using Immunomount (Thermo Fisher Scientific, Waltham, MA). Sections were imaged on an FV-3000 Olympus Microscope (Olympus America Inc, Center Valley, PA).

For wholemount immunohistochemistry, retinas were fixed in 4% paraformaldehyde, washed 4× with PBS and incubated with 20% sucrose solution overnight at 4°C. Retinas were incubated in blocking buffer for 1 hr and then with primary antibodies in blocking buffer added and incubated for 5 days at 4°C. Retinas were washed 4 times, 15 min each with PBX and incubated with blocking buffer for 1 hr, followed by overnight incubation at 4°C with secondary antibodies. Retinas were then washed 4× 15 min with PBX and mounted photoreceptors side up with Vectashield media and duct tape used as a spacer surrounding the retina. High magnification images were taken on a FV-3000 confocal microscope using 40× (NA =1.15) and 60× (NA = 1.45) objectives. Images were corrected for contrast and brightness using Flowview Software (Olympus, Waltham, MA). The number of rod synapses was estimated by counting mGluR6 puncta in whole mount images of immunohistochemically stained retina pieces that had been used to study the RGCs. LRIT3 and/or TRPM1 puncta also were counted. Two regions (70 μm × 70 μm) from each piece of retina used in MEA experiments were analyzed for mGluR6 and LRIT3 and/or TRPM1 puncta. Puncta were counted manually in whole mounts from maximum projections of z stacks that encompassed the entire outer plexiform layer (OPL).

rAAV Production and Injection—To express LRIT3 in rod photoreceptors we used a human rhodopsin (RHO) promoter to control expression in rAAVs (Allocca et al., 2007). The control virus expressed GFP under the control of the RHO promoter and is referred to as rAAV RHO::GFP. We created an LRIT3 expression construct by replacing the GFP with the

LRIT3 open reading frame (ORF, Accession # NM_001287224), and this is referred to as rAAV RHO::Lrit3. The expression construct was packaged in the rAAV2/2[MAX] capsid and virus produced as previously described (Reid et al., 2017; Reid and Lipinski, 2018). rAAVs were introduced into the retinas of postnatal day 5 (P5) mice after anesthesia by cooling on ice. rAAVs (0.6μl of 1×10^{13}vg/ml) were injected intravitreally. We also injected rAAV RHO::Lrit3 into the vitreous of P35 *Lrit3*$^{-/-}$ mice and 5 weeks later we recorded electroretinograms, removed the retinas and stained for LRIT3 and TRPM1 expression.

Electroretinography—Electroretinogram (ERG) recording methods have been described previously (Peachey et al., 2012). Mice were dark adapted overnight and anesthetized with ketamine/xylazine. All procedures to prepare the mice for ERGs were performed under dim red light. Pupil dilation and relaxed accommodation were achieved by applying 0.625% phenylephrine hydrochloride and 0.25% Tropicamide solutions to the corneal surface. Body temperature was maintained via an electric heating pad (TC1000 Temperature control, CWE Inc.). The cornea was treated with artificial tears (Tears Again, OCuSOFT, Gaithersburg, MD) and a clear acrylic contact lens with a gold electrode (LKC Technologies, Gaithersburg, MD) was placed. Ground and reference needle electrodes were placed in the tail and on the midline of the forehead, respectively, followed by a further 20 min dark adaptation. Full field flashes were presented bilaterally using an LKC Big Shot Ganzfeld (LKC Technologies, Gaithersburg, MD). Scotopic electroretinograms (ERGs) were obtained using an increasing intensity series of dim flashes presented on a dark background. Photopic ERGs were obtained after 5 min light adaption (20 cd.sec.m^{-2}) and presentation of a series of increasing intensity flashes on this background. The mice were recovered from the ERG procedure for at least 72 hours prior to assessing retinal ganglion cell (RGC) function on a multi-electrode array.

RGC recordings using Multi-Electrode Array (MEA)—The procedure of extracellular recordings of RGCs on the MEA have been previously described (Peachey et al., 2017). Briefly, mice were dark-adapted overnight, anesthetized with ketamine/xylazine and sacrificed by cervical dislocation. The anterior segments were removed and retinas were dissected under dim red light in oxygenated Ringer's solution. To remove the residual vitreous, the dissected retinas were incubated for 10 min in Ringers containing collagenase (240U/ml, cat # LS005273) and hyaluronidase (7200U/mL, cat # LS002592) (Worthington Biochemicals, Lakewood, NJ). Dorsal and ventral pieces of retina were dissected and placed on the MEA (60MEA200/30Ti; Multi Channel Systems, Reutlingen, Germany). The recording chamber was continuously perfused with oxygenated Ringer's solution at 36°C. The preparation was allowed to stabilize for 45 min in the dark before recording the spontaneous and visually evoked responses.

Visual stimuli were generated using custom code written in MATLAB (Mathworks, USA) and projected on to the retina through a mini-projector (HP Notebook Consumer projection Companion model #AX325AA). Scotopic responses were from 10 trials of full-field light stimuli (5 s duration; 20 s inter-stimulus interval, 1.49 cd/m^2) presented on to the dark-adapted retina. The retina was light adapted (3.01 cd/m^2) for 5 min and full-field light stimuli were presented (5 s duration; 20 s inter-stimulus interval, 303 cd/m^2) to obtain

photopic responses. Signals were band-pass filtered (80 –3,000 Hz) and digitized at 25 kHz (MC Rack software; Multi Channel Systems). A principle component analysis (Offline Sorter; Plexon, Dallas, TX) was used to sort the spike trains representing the activity of single RGC. Sorted units were exported to NeuroExplorer software (Nex Technologies, Madison, AL) for further analysis of spontaneous and evoked responses to each of the stimulus condition. An evoked response was defined as a response with a peak firing rate that was > +10 SEM above mean spontaneous rate. The response latency was defined as the time between stimulus onset and the peak maximum. The mean spontaneous rate was subtracted from the maximum firing rate to obtain the peak amplitude.

RGC Pharmacology—After recording spontaneous and visually evoked responses at three different scotopic intensities, synaptic blocker was added to the MEA bath solution to eliminate signaling through the ON pathway. We used the metabotropic glutamate receptor (mGluR6) agonist, L-2-Amino-4-phosphonobutyric acid (5μM;L-AP4 Tocris Bioscience) to block the synaptic transmission from photoreceptors to ON BCs (Slaughter and Miller, 1981). The synaptic blocker was applied for 15 min and full-field light stimuli (1.49 cd s/m2) were presented. A wash was performed for 15 min and visually evoked responses were recorded using the same full-field stimuli

QUANTIFICATION AND STATISTICAL ANALYSIS

Prism 8.0.2 software (Graphpad Software, Inc., La Jolla, CA) was used to perform the statistical analyses. When multiple post hoc tests were done, the p value was adjusted using the Bonferroni correction, and the p_{adj} reported. A p or $p_{adj} < 0.05$ was considered significant. The specific tests are described in detail in results and/or figure legends. All rAAV injected animals in which there was a normal ERG a-wave were included. Animals with injection induced microphthalmia were excluded from the analyses.

Supplementary Material

Refer to Web version on PubMed Central for supplementary material.

ACKNOWLEDGMENTS

This work was supported by funding from the NIH (R01 EY12354 to R.G.G., M.A.M., and N.H.) and an unrestricted grant from Research to Prevent Blindness to the University of Louisville. D.M.L. was supported through a Foundation for Fighting Blindness Individual Investigator Award (TA-NMT-0618-0739-MCW) and intramural funding through the Medical College of Wisconsin. R.G.G. holds the Preston Pope Joyes Endowed Chair in Biochemical Research, and M.A.M. holds the Kentucky Lions Research in Ophthalmology Endowed Chair.

REFERENCES

Agosto MA, Anastassov IA, Robichaux MA, and Wensel TG (2018). A large endoplasmic reticulum-resident pool of TRPM1 in retinal ON-bipolar cells. eNeuro 5, ENEURO.0143-18.2018.

Allocca M, Mussolino C, Garcia-Hoyos M, Sanges D, Iodice C, Petrillo M, Vandenberghe LH, Wilson JM, Marigo V, Surace EM, and Auricchio A (2007). Novel adeno-associated virus serotypes efficiently transduce murine photoreceptors. J. Virol 81, 11372–11380. [PubMed: 17699581]

Ball SL, Powers PA, Shin HS, Morgans CW, Peachey NS, and Gregg RG (2002). Role of the β(2) subunit of voltage-dependent calcium channels in the retinal outer plexiform layer. Invest. Ophthalmol. Vis. Sci 43, 1595–1603. [PubMed: 11980879]

Ball SL, Pardue MT, McCall MA, Gregg RG, and Peachey NS (2003). Immunohistochemical analysis of the outer plexiform layer in the nob mouse shows no abnormalities. Vis. Neurosci 20, 267–272. [PubMed: 14570248]

Bech-Hansen NT, Naylor MJ, Maybaum TA, Pearce WG, Koop B, Fishman GA, Mets M, Musarella MA, and Boycott KM (1998). Loss-of-function mutations in a calcium-channel alpha1-subunit gene in Xp11.23 cause incomplete X-linked congenital stationary night blindness. Nat. Genet 19, 264–267. [PubMed: 9662400]

Bech-Hansen NT, Naylor MJ, Maybaum TA, Sparkes RL, Koop B, Birch DG, Bergen AA, Prinsen CF, Polomeno RC, Gal A, et al. (2000). Mutations in NYX, encoding the leucine-rich proteoglycan nyctalopin, cause X-linked complete congenital stationary night blindness. Nat. Genet 26, 319–323. [PubMed: 11062471]

Cao Y, Posokhova E, and Martemyanov KA (2011). TRPM1 forms complexes with nyctalopin in vivo and accumulates in postsynaptic compartment of ON-bipolar neurons in mGluR6-dependent manner. J. Neurosci 31, 11521–11526. [PubMed: 21832182]

Cao Y, Sarria I, Fehlhaber KE, Kamasawa N, Orlandi C, James KN, Hazen JL, Gardner MR, Farzan M, Lee A, et al. (2015). Mechanism for selective synaptic wiring of rod photoreceptors into the retinal circuitry and its role in vision. Neuron 87, 1248–1260. [PubMed: 26402607]

Chang B, Heckenlively JR, Bayley PR, Brecha NC, Davisson MT, Hawes NL, Hirano AA, Hurd RE, Ikeda A, Johnson BA, et al. (2006). The nob2 mouse, a null mutation in Cacna1f: anatomical and functional abnormalities in the outer retina and their consequences on ganglion cell visual responses. Vis. Neurosci 23, 11–24. [PubMed: 16597347]

Demas J, Sagdullaev BT, Green E, Jaubert-Miazza L, McCall MA, Gregg RG, Wong RO, and Guido W (2006). Failure to maintain eye-specific segregation in nob, a mutant with abnormally patterned retinal activity. Neuron 50, 247–259. [PubMed: 16630836]

Gregg R, Lukasiewicz P, Peachey N, Sagdullaev B, and McCall M (2003). Nyctalopin is required for signaling through depolarizing bipolar cells in the murine retina. Invest. Ophthalmol. Vis. Sci 44, 4180.

Hasan N, Ray TA, and Gregg RG (2016). CACNA1S expression in mouse retina: novel isoforms and antibody cross-reactivity with GPR179. Vis. Neurosci 33, E009. [PubMed: 27471951]

Hasan N, Pangeni G, Ray TA, Fransen KM, Noel J, Borghuis BG, McCall MA, and Gregg RG (2018). LRIT3 is required for nyctalopin expression and normal ON and OFF pathway signaling in the retina. bioRxiv. 10.1101/431338.

Hoon M, Okawa H, Della Santina L, and Wong RO (2014). Functional architecture of the retina: development and disease. Prog. Retin. Eye Res 42, 44–84. [PubMed: 24984227]

Katiyar R, Weissgerber P, Roth E, Dörr J, Sothilingam V, Garcia Garrido M, Beck SC, Seeliger MW, Beck A, Schmitz F, and Flockerzi V (2015). Influence of the β2-subunit of L-type voltage-gated Cav channels on the structural and functional development of photoreceptor ribbon synapses. Invest. Ophthalmol. Vis. Sci 56, 2312–2324. [PubMed: 25766584]

Kerov V, Laird JG, Joiner ML, Knecht S, Soh D, Hagen J, Gardner SH, Gutierrez W, Yoshimatsu T, Bhattarai S, et al. (2018). $\alpha_2\delta$-4 is required for the molecular and structural organization of rod and cone photoreceptor synapses. J. Neurosci 38, 6145–6160. [PubMed: 29875267]

Mansergh F, Orton NC, Vessey JP, Lalonde MR, Stell WK, Tremblay F, Barnes S, Rancourt DE, and Bech-Hansen NT (2005). Mutation of the calcium channel gene Cacna1f disrupts calcium signaling, synaptic transmission and cellular organization in mouse retina. Hum. Mol. Genet 14, 3035–3046. [PubMed: 16155113]

Mussolino C, della Corte M, Rossi S, Viola F, Di Vicino U, Marrocco E, Neglia S, Doria M, Testa F, Giovannoni R, et al. (2011). AAV-mediated photoreceptor transduction of the pig cone-enriched retina. Gene Ther 18, 637–645. [PubMed: 21412286]

Neuillé M, El Shamieh S, Orhan E, Michiels C, Antonio A, Lancelot ME, Condroyer C, Bujakowska K, Poch O, Sahel JA, et al. (2014). Lrit3 deficient mouse (nob6): a novel model of complete congenital stationary night blindness (cCSNB). PLoS ONE 9, e90342. [PubMed: 24598786]

Neuillé M, Morgans CW, Cao Y, Orhan E, Michiels C, Sahel JA, Audo I, Duvoisin RM, Martemyanov KA, and Zeitz C (2015). LRIT3 is essential to localize TRPM1 to the dendritic tips of depolarizing

bipolar cells and may play a role in cone synapse formation. Eur. J. Neurosci 42, 1966–1975. [PubMed: 25997951]

Neuillé M, Cao Y, Caplette R, Guerrero-Given D, Thomas C, Kamasawa N, Sahel JA, Hamel CP, Audo I, Picaud S, et al. (2017). LRIT3 differentially affects connectivity and synaptic transmission of cones to ON- and OFF-bipolar cells. Invest. Ophthalmol. Vis. Sci 58, 1768–1778. [PubMed: 28334377]

Pardue MT, Ball SL, Candille SI, McCall MA, Gregg RG, and Peachey NS (2001). nob: A mouse model of CSNB1 In New Insights into Retinal Degenerative Diseases (Springer), pp. 319–328.

Peachey NS, Ray TA, Florijn R, Rowe LB, Sjoerdsma T, Contreras-Alcantara S, Baba K, Tosini G, Pozdeyev N, Iuvone PM, et al. (2012). GPR179 is required for depolarizing bipolar cell function and is mutated in autosomal-recessive complete congenital stationary night blindness. Am. J. Hum. Genet 90, 331–339. [PubMed: 22325362]

Peachey NS, Hasan N, FitzMaurice B, Burrill S, Pangeni G, Karst SY, Reinholdt L, Berry ML, Strobel M, Gregg RG, et al. (2017). A missense mutation in *Grm6* reduces but does not eliminate mGluR6 expression or rod depolarizing bipolar cell function. J. Neurophysiol 118, 845–854. [PubMed: 28490646]

Pearring JN, Bojang P Jr., Shen Y, Koike C, Furukawa T, Nawy S, and Gregg RG (2011). A role for nyctalopin, a small leucine-rich repeat protein, in localizing the TRP melastatin 1 channel to retinal depolarizing bipolar cell dendrites. J. Neurosci 31, 10060–10066. [PubMed: 21734298]

Pusch CM, Zeitz C, Brandau O, Pesch K, Achatz H, Feil S, Scharfe C, Maurer J, Jacobi FK, Pinckers A, et al. (2000). The complete form of X-linked congenital stationary night blindness is caused by mutations in a gene encoding a leucine-rich repeat protein. Nat. Genet 26, 324–327. [PubMed: 11062472]

Ray TA (2013). Constructing the rod bipolar signalplex using animal models of retinal dysfunction. Electronic Theses and Dissertations, Paper 1188. 10.18297/etd/1188.

Reid CA, and Lipinski DM (2018). Small and micro-scale recombinant adeno-associated virus production and purification for ocular gene therapy applications. Methods Mol. Biol 1715, 19–31. [PubMed: 29188503]

Reid CA, Ertel KJ, and Lipinski DM (2017). Improvement of photoreceptor targeting via intravitreal delivery in mouse and human retina using combinatory rAAV2 capsid mutant vectors. Invest. Ophthalmol. Vis. Sci 58, 6429–6439. [PubMed: 29260200]

Rentería RC, Tian N, Cang J, Nakanishi S, Stryker MP, and Copenhagen DR (2006). Intrinsic ON responses of the retinal OFF pathway are suppressed by the ON pathway. J. Neurosci 26, 11857–11869. [PubMed: 17108159]

Sarria I, Cao Y, Wang Y, Ingram NT, Orlandi C, Kamasawa N, Kolesnikov AV, Pahlberg J, Kefalov VJ, Sampath AP, and Martemyanov KA (2018). LRIT1 modulates adaptive changes in synaptic communication of cone photoreceptors. Cell Rep 22, 3562–3573. [PubMed: 29590623]

Scalabrino ML, Boye SL, Fransen KM, Noel JM, Dyka FM, Min SH, Ruan Q, De Leeuw CN, Simpson EM, Gregg RG, et al. (2015). Intravitreal delivery of a novel AAV vector targets ON bipolar cells and restores visual function in a mouse model of complete congenital stationary night blindness. Hum. Mol. Genet 24, 6229–6239. [PubMed: 26310623]

Schroeder A, and de Wit J (2018). Leucine-rich repeat-containing synaptic adhesion molecules as organizers of synaptic specificity and diversity. Exp. Mol. Med 50, 10. [PubMed: 29628503]

Schroeder A, Vanderlinden J, Vints K, Ribeiro LF, Vennekens KM, Gounko NV, Wierda KD, and de Wit J (2018). A modular organization of LRR protein-mediated synaptic adhesion defines synapse identity. Neuron 99, 329–344.e7. [PubMed: 29983322]

Slaughter MM, and Miller RF (1981). 2-Amino-4-phosphonobutyric acid: a new pharmacological tool for retina research. Science 211, 182–185. [PubMed: 6255566]

Soto F, Watkins KL, Johnson RE, Schottler F, and Kerschensteiner D (2013). NGL-2 regulates pathway-specific neurite growth and lamination, synapse formation, and signal transmission in the retina. J. Neurosci 33, 11949–11959. [PubMed: 23864682]

Soto F, Zhao L, and Kerschensteiner D (2018). Synapse maintenance and restoration in the retina by NGL2. eLife 7, e30388. [PubMed: 29553369]

Strom TM, Nyakatura G, Apfelstedt-Sylla E, Hellebrand H, Lorenz B, Weber BH, Wutz K, Gutwillinger N, Rüther K, Drescher B, et al. (1998). An L-type calcium-channel gene mutated in incomplete X-linked congenital stationary night blindness. Nat. Genet 19, 260–263. [PubMed: 9662399]

Ueno A, Omori Y, Sugita Y, Watanabe S, Chaya T, Kozuka T, Kon T, Yoshida S, Matsushita K, Kuwahara R, et al. (2018). Lrit1, a retinal transmembrane protein, regulates selective synapse formation in cone photoreceptor cells and visual acuity. Cell Rep 22, 3548–3561. [PubMed: 29590622]

Vardi N, Duvoisin R, Wu G, and Sterling P (2000). Localization of mGluR6 to dendrites of ON bipolar cells in primate retina. J. Comp. Neurol 423, 402–412. [PubMed: 10870081]

Waldner DM, Bech-Hansen NT, and Stell WK (2018). Channeling vision: CaV1.4—a critical link in retinal signal transmission. BioMed Res. Int 2018, 7272630. [PubMed: 29854783]

Wang Y, Fehlhaber KE, Sarria I, Cao Y, Ingram NT, Guerrero-Given D, Throesch B, Baldwin K, Kamasawa N, Ohtsuka T, et al. (2017). The auxiliary calcium channel subunit α2δ4 is required for axonal elaboration, synaptic transmission, and wiring of rod photoreceptors. Neuron 93, 1359–1374.e6. [PubMed: 28262416]

Highlights

- The LRR protein LRIT3 is expressed in rod photoreceptors
- rAAV-expressed LRIT3 in rod photoreceptors localizes correctly to the synapse
- LRIT3 expression in rods restores TRPM1 expression in postsynaptic bipolar cells
- Dark-adapted RGC function is restored in LRIT3 KO mice by LRIT3 expression in rods

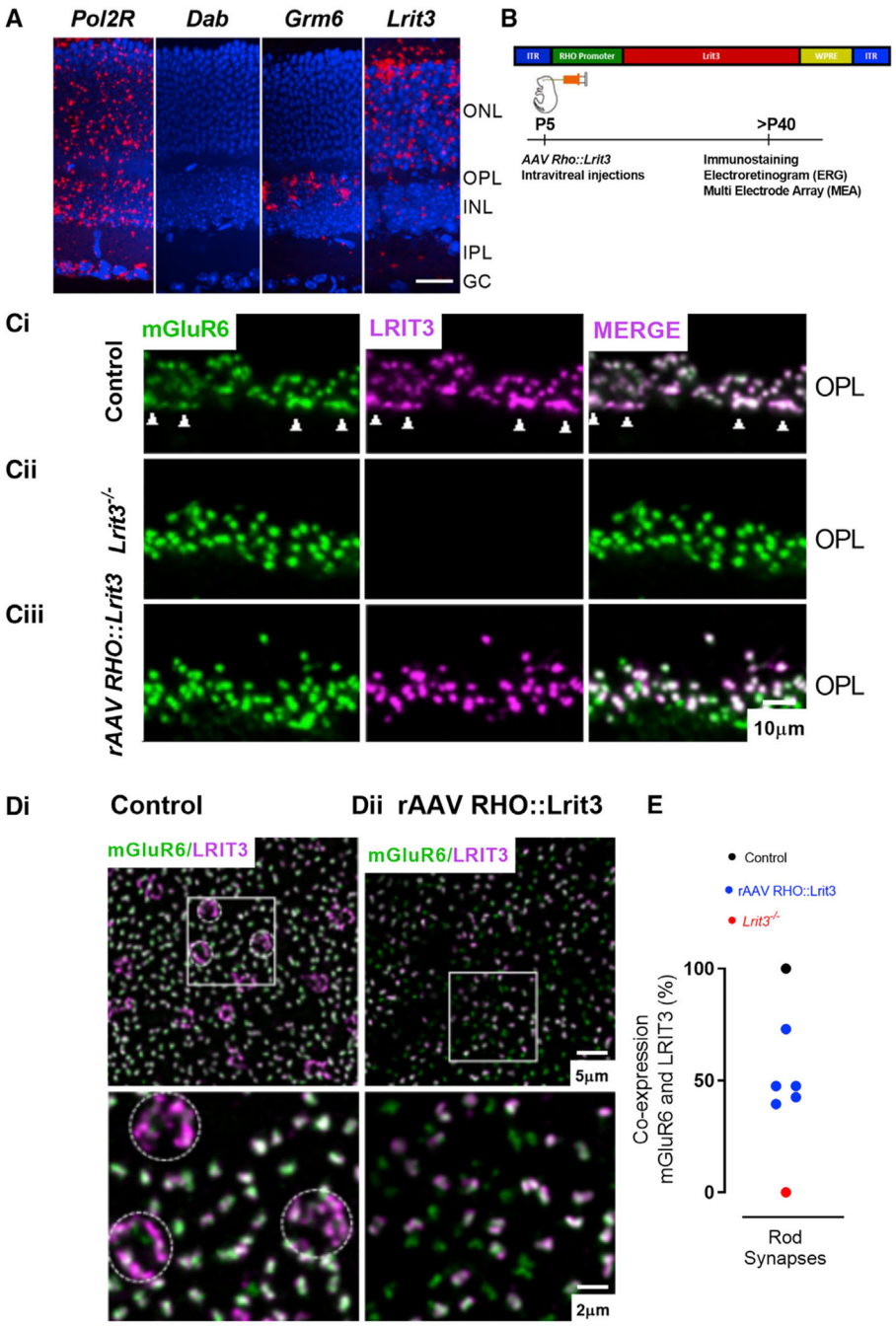

Figure 1. LRIT3 Is Expressed in Rods

(A) *In situ* hybridization for mRNA probes in transverse retinal sections shows that the positive control, *Pol2r*, is ubiquitously expressed throughout all retinal layers. *Grm6* expression is found in the outer part of the inner nuclear layer (INL), where the cell bodies of the ON BCs are located. *Dab*, the negative control shows no expression; *Lrit3* expression is found almost exclusively in the outer nuclear layer (ONL), where the photoreceptor cell bodies are located. GCL, ganglion cell layer. DAPI stain nuclei (blue) and mRNA probes (red). Scale bar, 20 µm.

(B) Schematic diagram of the rAAV RHO::Lrit3 vector (top) and the time course of treatment and analyses (bottom).

(C) Transverse retinal sections of control (i), *Lrit3*$^{-/-}$ (ii), and rAAV RHO::Lrit3-treated *Lrit3*$^{-/-}$ (iii) retinas stained for mGluR6 (green) and LRIT3 (magenta). Arrowheads in (i) indicate cone terminal staining. OPL, outer plexiform layer. Scale bar, 10 μm.

(D) Whole mounts imaged at the level of the OPL from control (i) and rAAV RHO::Lrit3-treated *Lrit3*$^{-/-}$ (ii) retinas stained for mGluR6 (green) and LRIT3 (magenta). Dotted circles in (i) indicate cone terminals. Boxed region is enlarged below. Note the absence of cone terminal staining in the rAAV RHO::Lrit3-treated *Lrit3*$^{-/-}$ retina (ii).

(E) Quantification of the percentage of rod synapses expressing LRIT3 in control, *Lrit3*$^{-/-}$, and rAAV RHO::Lrit3-treated *Lrit3*$^{-/-}$ (n = 5 eyes, 5 mice).

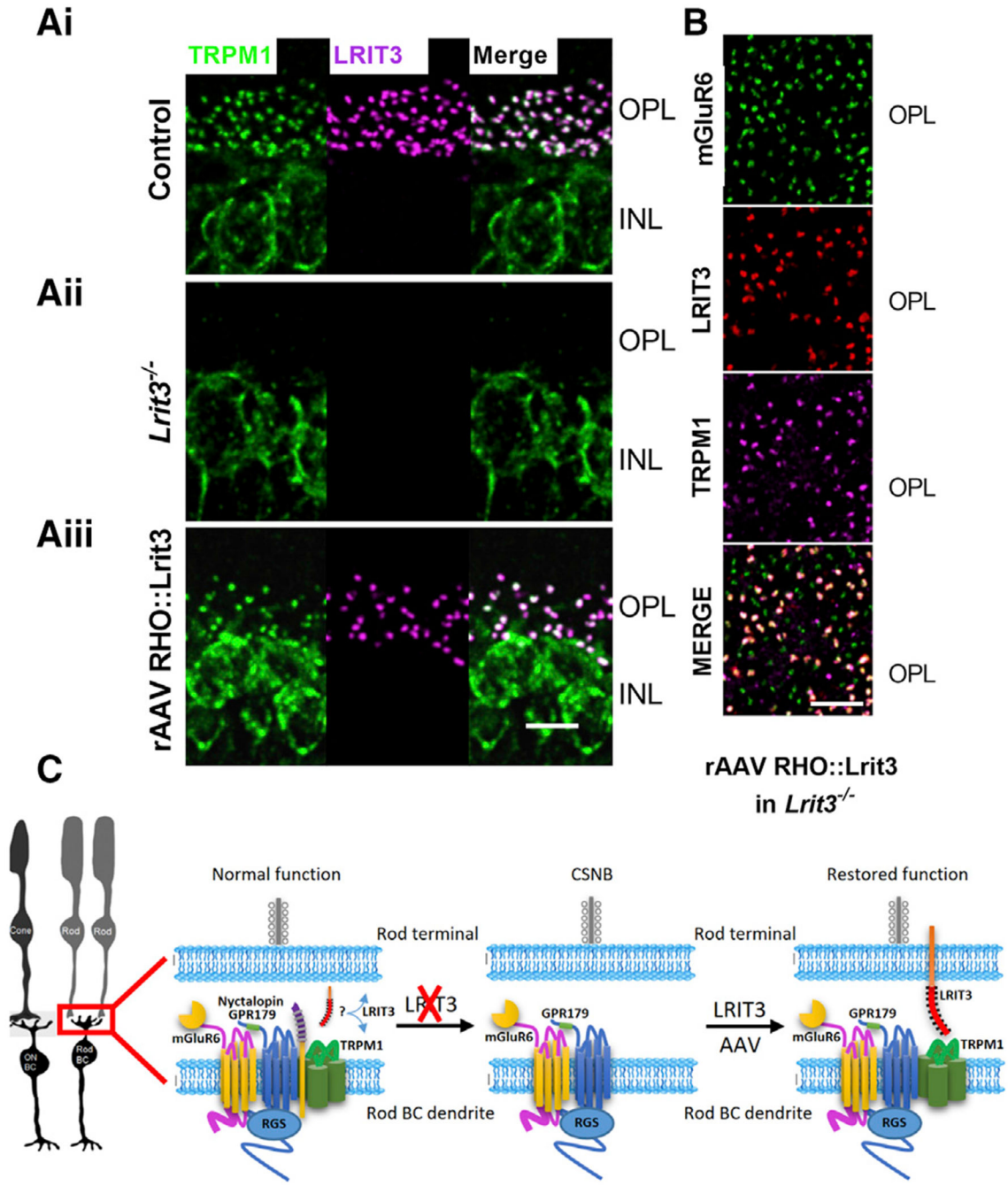

Figure 2. LRIT3 Expression in *Lrit3*$^{-/-}$ Rods Restores Expression of TRPM1 to the Dendrites of RBCs in the Outer Plexiform Layer

(A) Transverse retinal sections of control (i), *Lrit3*$^{-/-}$ (ii), and rAAV RHO::Lrit3-treated *Lrit3*$^{-/-}$ (iii) retinas stained for TRPM1 (green) and LRIT3 (magenta). Scale bar, 10 μm. (B) Whole mount imaged at the level of the OPL of a retina from a rAAV RHO::Lrit3-treated *Lrit3*$^{-/-}$ mouse stained for mGluR6 (green), LRIT3 (red), and TRPM1 (magenta). Note that TRPM1 expression co-localizes with both LRIT3 and mGluR6 but is absent when LRIT3 is absent. Scale bar, 20 μm.

(C) Schematic of the normal postsynaptic elements in RBPs, indicating an unknown location for LRIT3, the impact on this complex of the loss of LRIT3, and the consequence of restoring LRIT3 expression to rod photoreceptors.

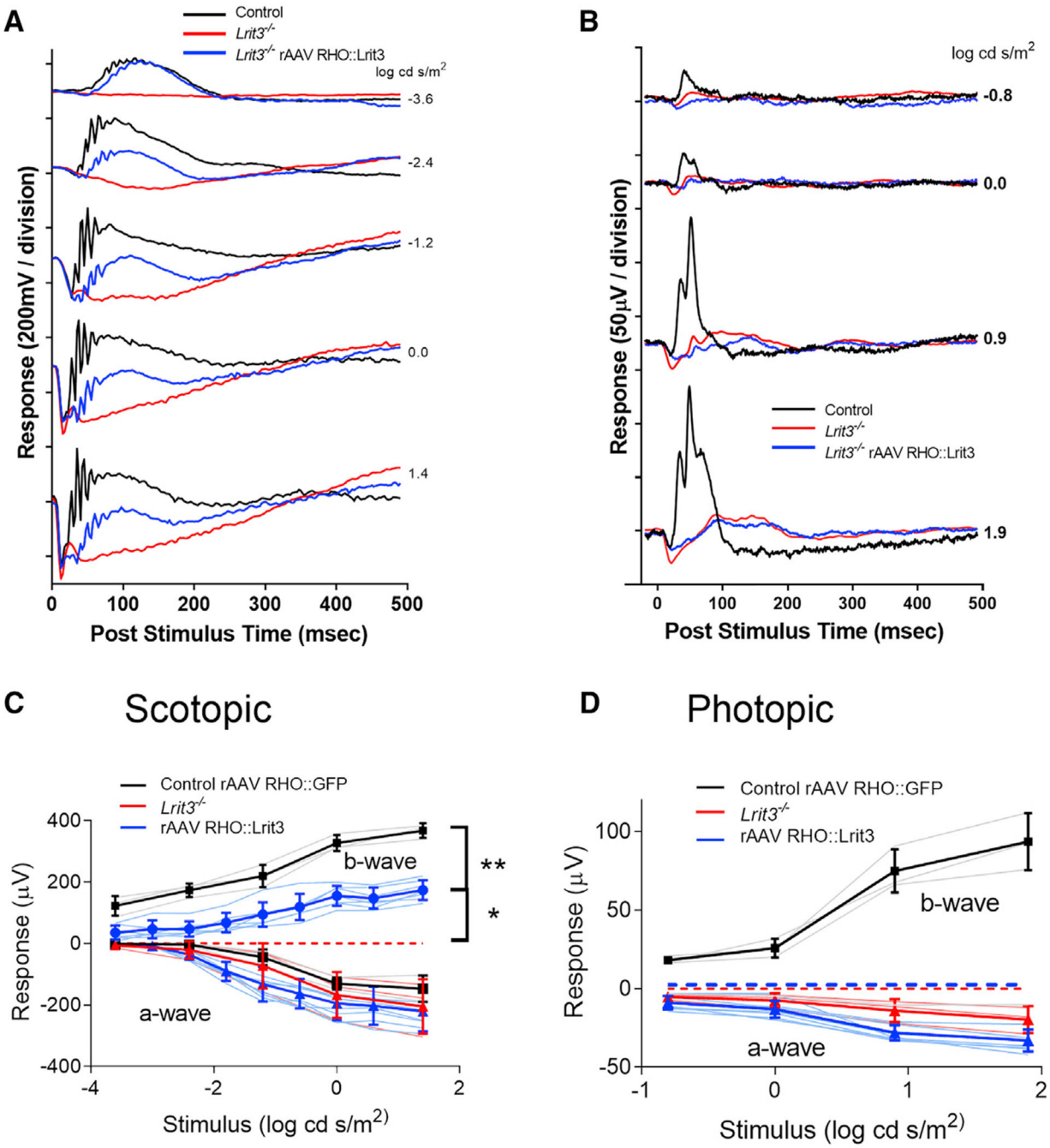

Figure 3. LRIT3 Expression in *Lrit3*$^{-/-}$ Rods Restores RBC Function

(A and B) Scotopic (A) and photopic (B) electroretinograms at different stimulus intensities for one control eye (black), an age-matched *Lrit3*$^{-/-}$ eye (red), and an rAAV RHO::Lrit3-treated *Lrit3*$^{-/-}$ eye (blue).

(C and D) Average stimulus-response plots for the ERG b-wave amplitude under scotopic (C) and photopic (D) conditions for control rAAV RHO::GFP (n = 3, black), *Lrit3*$^{-/-}$ (n = 3, red), and rAAV RHO::Lrit3-injected *Lrit3*$^{-/-}$ (n = 8, blue). Pale lines are the responses for

individual eyes, and dark lines are the mean ± SD for each group. The dashed red and blue lines indicate no b-wave (zero amplitude) in these animals.

Statistics: (C) comparison of control versus rAAV RHO::LRIT3 groups, $^{**}p_{adj} < 0.01$ for stimuli, two-way repeated-measures ANOVA; comparison of rAAV RHO::LRIT3-injected *Lrit3*$^{-/-}$ versus *Lrit3*$^{-/-}$ groups (b-wave amplitude = 0), $^{*}p_{adj} < 0.03$ for all stimuli compared using single-sample t test adjusted for multiple comparisons by Bonferroni correction. There are no differences in a-wave amplitude between groups under either scotopic or photopic conditions (two-way repeated-measures ANOVA, $p_{adj} > 0.05$). p_{adj}, adjusted p value.

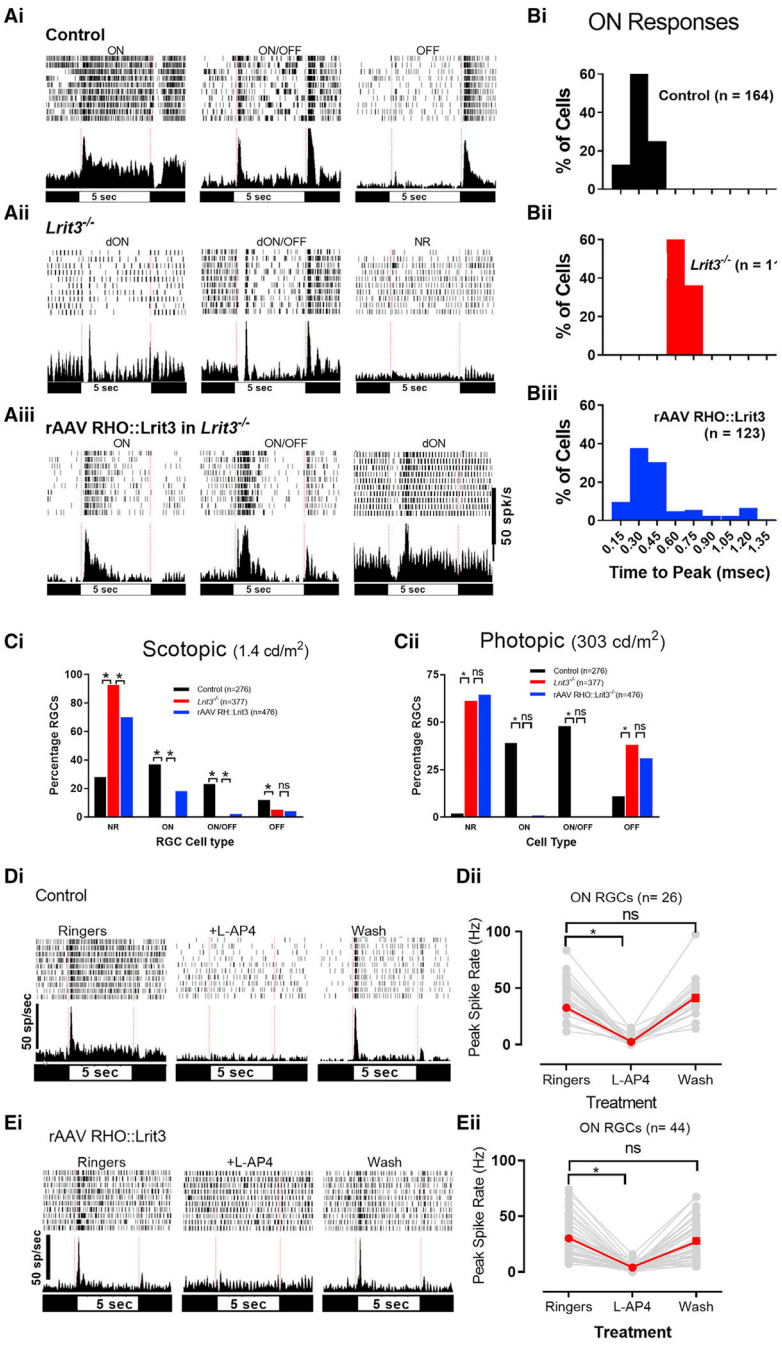

Figure 4. LRIT3 Expression in Rods Restores Normal ON RGC Function in *Lrit3*$^{-/-}$ Retinas

(A) Example of raster plots and peri-stimulus time histograms (PSTH) of each cell type as indicated, recorded on the MEA (multi-electrode array).

(B) Frequency distribution of time to peak (TTP) for the ON responses in control (i), *Lrit3*$^{-/-}$ (ii), and rAAV RHO::Lrit3-treated *Lrit3*$^{-/-}$ (iii) retinas.

(C) Percentage of each cell type recorded under scotopic (i) and photopic (ii) conditions. dON and dON/OFF cells are omitted because of their small numbers, but see Table S1 for numbers. All groups were analyzed using chi-square tests, and when significant ($p < 0.05$)

two-way post hoc tests were done (chi-square) with Bonferroni adjustment of the p values for multiple testing (*$p_{adj} < 0.025$).

(D and E) Example PSTH's for a cell from control (Di) and rAAV RHO::Lrit3 retinas (Ei) in Ringer's solution, in Ringer's plus 5 mM L-AP4, and after L-AP4 washout. (Dii) The peak responses for individual cells (gray lines) and mean ± SEM (red lines) of control (Dii) and rAAV RHO::Lrit3-treated *Lrit3*$^{-/-}$ (Eii) retinas are shown. The response amplitudes in (D) and (E) in L-AP4 was significantly decreased (*$p_{adj} < 0.0001$, repeated-measures ANOVA, Bonferroni corrected for both datasets) and after washout was not significant (ns; $p_{adj} > 0.4$). p_{adj}, adjusted p value.

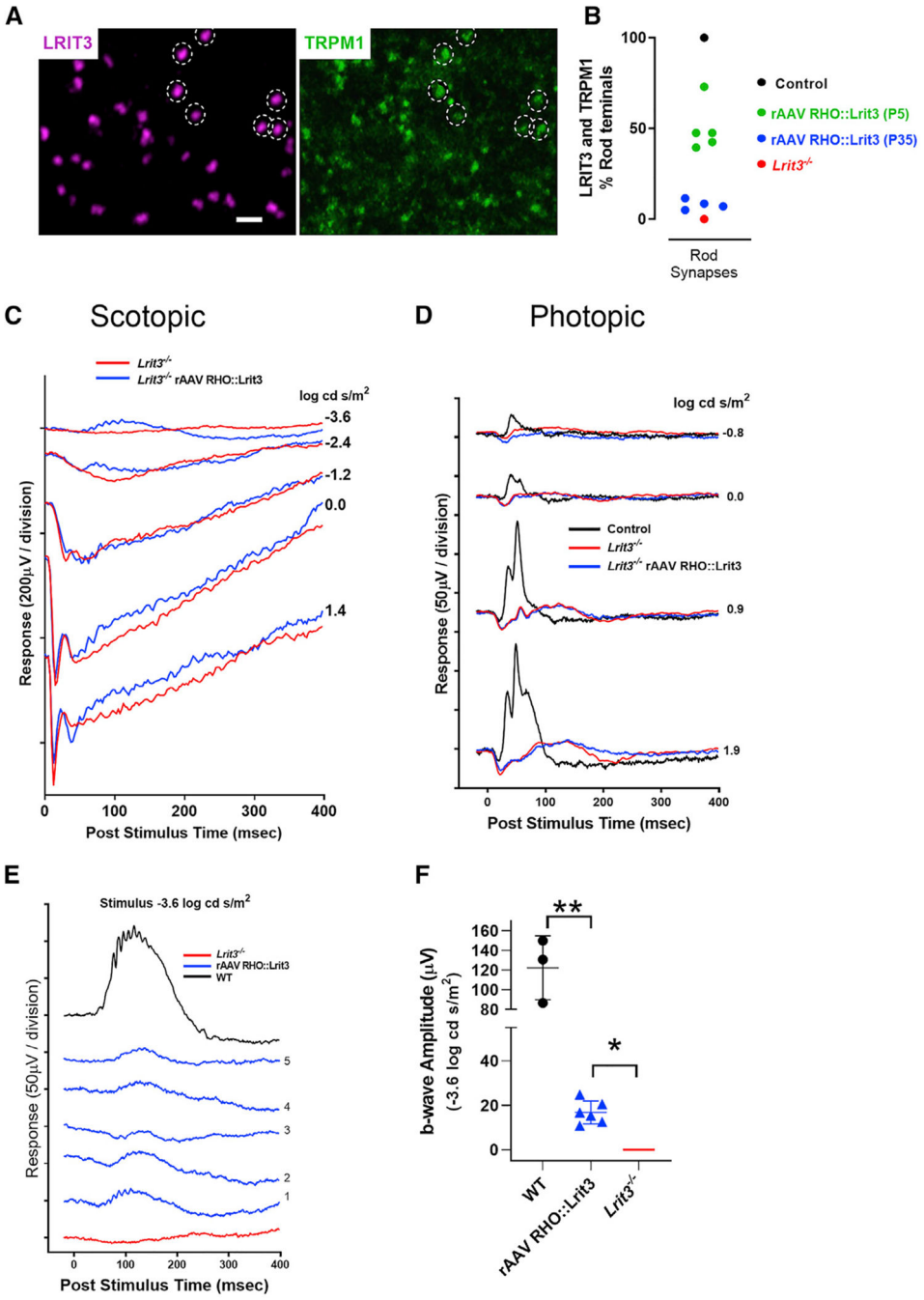

Figure 5. LRIT3 Expression in Rods of Adult *Lrit3*$^{-/-}$ Mice Restores RBC Function

(A) Whole mount of retinas from P35 rAAV RHO::Lrit3-treated *Lrit3*$^{-/-}$ mice stained for LRIT3 (magenta) and TRPM1 (green) analyzed at P70. A sample of the LRIT3 puncta is highlighted (dashed circles), showing that they co-localize with TRPM1. Every LRIT3 puncta co-localizes with TRPM1 puncta. Scale bar, 2 μm.

(B) Quantification of the percentage of rod synapses expressing LRIT3 and TRPM1 in WT (black symbol), rAAV RHO::Lrit3-injected animals at P5 (green symbol) or P35 (blue

symbol), and *Lrit3*$^{-/-}$ retinas (red symbol). Note that the P5 data are replicated from Figure 1.

(C and D) Scotopic (C) and photopic (D) electroretinograms at different stimulus intensities for one control eye (black), an age-matched *Lrit3*$^{-/-}$ eye (red), and an rAAV RHO::Lrit3-treated *Lrit3*$^{-/-}$ P35 mouse eye (blue).

(E) Scotopic responses to a −3.6 log cd s/m^2 stimulus for a control rAAV RHO::GFP (black), a *Lrit3*$^{-/-}$ (red), and five rAAV RHO::Lrit3-injected P35 *Lrit3*$^{-/-}$ (blue) mouse eyes.

(F) Response amplitudes from the five animals in (E) (blue triangles) and WT (black circles) to the −3.6 log cd s/m^2 stimuli. The red line indicates no b-wave (zero amplitude) in the *Lrit3*$^{-/-}$ animals (mean ± SD are indicated. The WT data are from Figure 3C.

Statistics: (F) rAAV RHO::Lrit3-injected *Lrit3*$^{-/-}$ eyes show significantly greater b-waves than *Lrit3*$^{-/-}$ groups (b-wave amplitude = 0), *$p < 0.01$ (single-sample t test). rAAV RHO::Lrit3-injected *Lrit3*$^{-/-}$ eyes show significantly smaller b-waves than WT eyes, **$p < 0.001$ (two-sided t test).

KEY RESOURCES TABLE

REAGENT or RESOURCE	SOURCE	IDENTIFIER
Antibodies		
Guinea pig anti-LRIT3	Ronald Gregg, Hasan et. al. (2018)	N/A
Rabbit anti-TRPMI	Ronald Gregg; Hasan et. al. (2018)	N/A
Sheep anti-mGluR6	Kiril Martemyanov; Cao et. al. 2011	N/A
Donkey anti-sheep IgG-AlexaFluor 488	Life Technologies	Cat # A111015
Donkey anti-rabbit IgG-AlexaFluor 647	Life Technologies	Cat # A31573
Donkey anti-guinea pig IgG-Cy3	Millipore	Cat # AP193C
Donkey anti-rabbit IgG-AlexaFluor 488	Life Technologies	Cat# A21206
Bacterial and Virus Strains		
pAAV-RHO::Lrit3	This paper	Addgene; Cat # 126511
rAAV2/2[MAX] capsid	Reid et al., 2017	N/A
Critical Commercial Assays		
In-Fusion® HD Cloning Plus	Takara	Cat # 638910
Experimental Models: Organisms/Strains		
Mouse: Lrit3^{em1Rgg}	Ronald Gregg	MGI: 5645054
C57BL/6J	Jackson Labs	Stock # 000664; RRID:IMSR_JAX:000664
Oligonucleotides		
Lrit3 KO genotyping forward	CTTTAAACGGAGTCTCGAAGC	N/A
Lrit3 KO genotyping reverse	CTGACCGCCTCGTTTGGCAC	N/A
Software and Algorithms		
Prism 8.1.0 (325)	Graphpad Software	RRID:SCR_002798
MC_Rack 4.6.2	Multi Channel System	RRID:SCR_014955
Offline Sorter 3.3.5	Plexon Inc	RRID:SCR_000012
NeuroExplorer 5.103	Nex Technologies	RRID:SCR_001818
Fluoview	Olympus	RRID:SCR_017015
Other		
RNAScope® *in situ* hybridization	Grm6; Genbank:NM_173372.2	N/A
RNAScope® *in situ* hybridization	Mm-Pol2ra ; positive control	Cat # 312471
RNAScope® *in situ* hybridization	DapB ; negative control	Cat # 310043